Proceedings of the ASME Turbo Expo 2016
GT2016
June 13-17, 2016, Seoul, South Korea

GT2016-56460

IMPACT OF SWIRLING FLOW STRUCTURE ON SHEAR LAYER VORTICITY FLUCTUATION MECHANISMS

Benjamin Mathews, Samuel Hansford*, Jacqueline O'Connor
Pennsylvania State University
University Park, Pennsylvania, USA

ABSTRACT

Vorticity fluctuations have been identified as an important coupling mechanism during velocity-coupled combustion instability in swirl-stabilized flames. Acoustic oscillations in the combustor can cause all components of vorticity to oscillate, particularly the cross-stream, or azimuthal, vorticity that is excited in shear layer roll-up, and streamwise, or axial, vorticity that is excited during swirl fluctuations. These fluctuations can be induced by longitudinal acoustic fluctuations that oscillate across the swirler and dump plane upstream of the flame. While these fluctuations have been identified in a number of configurations, the sensitivity of this mechanism to flow configuration and boundary conditions has not been studied parametrically. In this study, we investigate the impact of time-averaged swirl level, confinement, and forcing frequency and amplitude on vorticity fluctuation dynamics in the azimuthal direction of a non-reacting swirling jet. The goal of this work is to better understand the dependence of vorticity fluctuations on these parameters as well as the vorticity conversion processes that occur in the flow. We have shown that vorticity fluctuation levels vary with time-averaged swirl number, particularly in the presence of a self-excited precessing vortex core, which dampens most acoustically-driven motion. Additionally, variations in forcing frequency excite flow response in different portions of the flow, particularly for different swirl numbers. Finally, confinement drastically changes the flow topology and unforced dynamics, resulting in significantly different response to forcing and generation of vortical fluctuations.

* Corresponding Author Email: seh304@psu.edu, jxo22@engr.psu.edu

NOMENCLATURE

D	Nozzle diameter
L^*	Convective wavelength
S	Swirl number
f	Frequency
r	Radial coordinate
t	Time
u	Velocity
x	Axial coordinate
θ	Azimuthal coordinate
ω	Vorticity

Superscripts

-	Time-averaged quantity
‘	Fluctuation quantity
~	Harmonically reconstructed quantity
^	Fourier transformed quantity

Subscripts

a	Acoustic
ff	Forcing frequency
rms	Root mean squared
x	Axial component
θ	Azimuthal component
ω	Vortical contribution

Acronyms

PIV	Particle image velocimetry
PVC	Precessing vortex core
SNR	Signal-to-noise ratio

INTRODUCTION

Pollutant emissions from combustion processes are of great public concern due to their impact on health and the environment, and the issue of climate change has only heightened these concerns. The majority of new power generation gas turbines contain fuel-lean premixed combustors in an effort to reduce these emissions, particularly NO_x [1]. Unfortunately, these systems are also more susceptible to combustion instabilities.

Combustion instability is a coupling between pressure and heat release rate oscillations in the combustion chamber, and it occurs at distinct frequencies and amplitudes that are determined by the combustor geometry and operating condition [2]. Combustion instabilities can lead to a number of operational and structural problems in engines [3]. Considerable effort has been made to understand the different types of coupling mechanisms between acoustics and heat release rate oscillations in an attempt to prevent combustion instabilities.

The two dominant coupling mechanisms of flame response in lean premixed combustor systems are fluctuations in the fuel to air ratio and velocity fluctuations, which are comprised of both acoustic and vortical disturbances [4]. In this work, we focus on the velocity coupling mechanism. Acoustic velocity fluctuations oscillate with the acoustic field, which in this study is longitudinal. Vortical disturbances are generated by modulation of separating shear layers, including those generated in the swirler and at the dump plane. These vortical fluctuations propagate downstream at roughly the mean convective speed and interact with the flame, causing wrinkles that result in oscillations in heat release rate, which can feed more energy into the acoustic modes of the system.

Vortex roll-up in the shear layers, generated at the separation point of the dump plane, has been studied extensively in the combustion instability literature. This mechanism is seen in a number of combustor configurations, including backwards facing steps [5-7], bluff-body stabilized flames [8-11], as well as swirl-stabilized combustors [12-18]. Swirling flows have both axial and azimuthal shear layers, the former of which is a consequence of the addition of swirl. Additionally, when vortex breakdown occurs there are both inner and outer shear layers. Vortical roll-up in the shear layers is caused by the Kelvin-Helmholtz instability mechanism. The flame stabilizes one or both of the shear layers and large scale eddies in the shear layer periodically wrinkle the flame. The dominant flow-flame coupling mechanism is through flame wrinkling, which alters the flame surface area and changes the global heat release rate [19]. Stretch-driven coupling between vortices and flame heat release rate is present at high frequencies and typically not a significant contribution to overall flame heat release rate oscillations [20, 21].

Additionally, there exists an indirect coupling mechanism that is unique to swirling flows. In this mechanism, acoustic waves, propagating through the swirler, generate azimuthal velocity fluctuations that are convected by the flow. These azimuthal velocity fluctuations interact with the flame, causing oscillations in heat release rate. In particular, oscillations in swirl number can result in oscillations in flame angle, creating "base waves" or "root waves" that travel along the flame. Experimental investigations on the impact of swirl fluctuations due to acoustic forcing and the effects on flame dynamics have been undertaken by a number of researchers [12, 22, 23]. Computational studies have further developed the understanding of this disturbance mechanism [24, 25].

One of the common results of these aforementioned studies is that the amplitude and relative contribution of the vorticity fluctuation mechanism to the overall combustion instability is strongly dependent on the flow geometry and operating condition. For example, vortex roll-up in the shear layers is a function of shear layer receptivity (which is dependent on shear layer thickness and Reynolds number [26]), and axial swirl fluctuations can vary with swirl strength and combustor expansion ratio [27]. O'Connor and Lieuwen proposed a transfer function approach to describing the coupling between acoustic fluctuations and vortical fluctuations in combustion systems [28]. In this study, we make parametric measurements of this transfer function for a variety of swirl numbers and forcing frequencies to begin to identify key trends in flow receptivity that lead to the coupling between acoustic and vortical motion in combustors, both of which eventually drive heat release rate oscillations.

The results of this work can be used in a number of ways. First, understanding the receptivity of the shear layers to acoustic oscillations can provide better understanding of the coupling between acoustic fields and flame heat release rate oscillations during a thermoacoustic instability. Moreover, it may help influence the design of future combustion systems so as to dampen the receptivity of the shear layers to acoustic excitation, resulting in lower flame heat release rate oscillations from velocity-coupled mechanisms. Finally, these results can be used as inputs to reduced-order flame response models, such as level-set formulations, where velocity fields are specified and flame response is calculated [19, 21, 24, 25]. These models have been shown to reproduce experimental flame response data with accuracy by capturing key flame physics in the model; the transfer function approach proposed by O'Connor and Lieuwen and measured in this study identifies what these key flame physics actually are.

The remainder of the paper is organized as follows. First, we present the experimental design of our longitudinally forced, swirl stabilized combustor. Next, we examine the time-averaged behavior of the jet at seven swirl levels to illustrate the progression of the flow field. Then, we identify the response of the jet to acoustic forcing at each unique swirl level by examining the fluctuating vorticity response at the specific forcing frequency. Lastly, we relate the vorticity response to the incoming velocity fluctuations at the nozzle and present measurements of the vorticity transfer function for various swirl levels and forcing conditions in order to identify flow receptivity to acoustic forcing.

EXPERIMENTAL OVERVIEW

The experimental facility used in this study is shown in Figure 1. There are three main components to this facility: (i) the two microphone injector nozzle, (ii) the swirler chamber with a variable, radial-entry swirler, and (iii) the settling chamber with longitudinal acoustic forcing. The incoming air enters the 15.25 cm diameter settling chamber where two perforated plates breakup large-scale, incoming turbulence. There are two speakers at the base of the facility that provide longitudinal forcing.

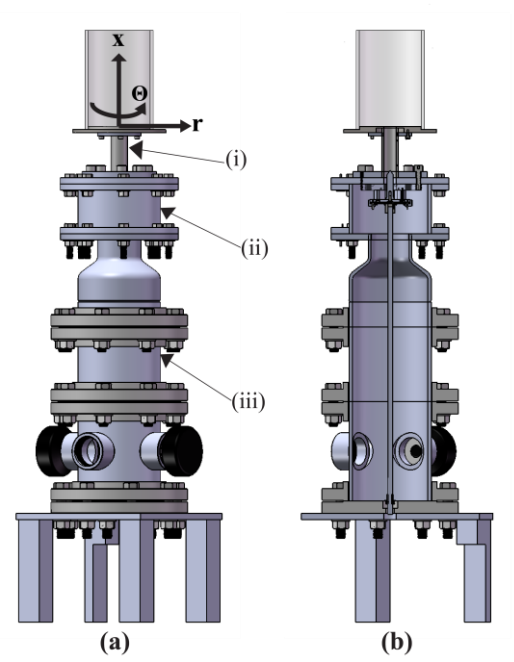

Figure 1: (a) Swirling flow facility with two microphone injector and (b) cut-away to show the location of the variable swirler section.

The flow enters at the base of the experiment, flows into the swirler chamber, and then passes through the variable-angle, radial-entry swirler. The swirler consists of eight NACA 0025 airfoils that are 2.54 cm tall and have a chord length of 2.54 cm. A stepper motor beneath the experiment can rotate the airfoil blades between 65º and -65º with a resolution of 2.5º. A positive blade angle produces a counter-clockwise rotating swirl motion (positive azimuthal velocity) and a negative blade angle produces clockwise rotating swirl (negative azimuthal velocity). After the flow passes through the swirler, the flow is turned upwards by a centerbody, which contracts to a point 8.9 cm upstream of the nozzle exit. The flow exits through a 2.54 cm nozzle into the combustion chamber. As shown in Figure 1, the combustion chamber is circular and has a diameter of 15.25 cm and is 20.3 cm in length. For the first part of this study, the flow field is unconfined; the second portion of this work considers the effects of confinement on the flow behavior.

Diagnostic Techniques

Speakers at the base of the experiment provide longitudinal acoustic forcing, and forcing is performed at two frequencies, 600 and 1800 Hz, at different acoustic amplitudes. The two microphone method is used to measure the acoustic velocity fluctuations inside the injector. The pressure transducers are located 2.54 cm and 7.62 cm downstream of the swirler, and 6.92 cm and 1.84 cm from the nozzle exit, respectively. The separation distance, 5.08 cm, was determined using guidance from Åbom and Boden [29]**.** The pressure transducers used in this experiment are PCB Model 113B28. The output signal from the pressure transducers is amplified by a PCB signal conditioner/amplifier and is recorded using a National Instruments analog voltage input module. The signal conditioner gain is varied depending on the flow conditions; for the non-precessing vortex core cases the gain is 25, whereas when a precessing vortex core (PVC) is present the gain is 10. The pressure sensor sampling rate is 20 kHz with a run time of 3 seconds. The voltage signal is ensemble averaged for a spectral resolution of 5 Hz. The acoustic velocity fluctuations are normalized by the bulk flow velocity, which is calculated from a Thermal Instruments thermal mass flow meter model 600-9 that is also sampled at 20 kHz for 3 seconds. The flow rate is maintained within 1 SCFM of 30 SCFM, which corresponds to a bulk flow velocity of 28 m/s and Reynolds number of 35,000. Additionally, there is no preheating so the incoming air has a temperature of roughly 293 K.

Stereo particle image velocimetry (PIV) is utilized to record the three-dimensional velocity field. PIV measurements are taken in the *x*-*r* plane where the radial and axial velocities are in-plane, whereas the azimuthal velocity is through the laser plane. A Hawk/Darwin Duo Nd-YAG, 532 nm wavelength, 60 W laser is used for PIV. For the 15º, 50º, and 65º blade angles, an SA5 and SA1.1 Photron CMOS high speed cameras are used in a forward-backward configuration while for the other four swirl conditions, two SA5 Photron CMOS cameras are used in a forward-forward configuration. The sampling rate is 5 kHz with a time separation of 25 μs and 5000 images are taken for a spectral resolution of 1 Hz. Aluminum oxide particles with a nominal diameter of 1-2 μm are used as tracer particles and can accurately follow flow perturbations up to a frequency of 4000 Hz [30]**.** Velocity vectors are calculated in DaVis 8.2.3 without any pre-processing or masking. Stereo cross-correlation with multi-pass iterations with decreasing window sizes is used. The first pass is a 32x32 pixel interrogation window with a 50% overlap followed by 2 passes with a 16x16 pixel interrogation with a 50% overlap. During vector post-processing there are two methods used to reject vectors. First, if the vector is more than 3 times the RMS of the surrounding vectors, the vector is removed and replaced. Additionally, universal outlier detection removes and replaces spurious vector results. The percentage of first and second choice vectors are 79% and 10%, respectively.

Data Analysis

A harmonic reconstruction technique is used to quantify the dynamic vortical response of the flow field to the acoustic perturbations at the forcing frequency. The azimuthal vorticity is calculated by taking the curl of the in-plane velocity field and the mean is subtracted to determine the fluctuating azimuthal vorticity. A Fourier transform is applied to the fluctuating azimuthal vorticity field and the complex, Fourier-transformed, azimuthal vorticity oscillation at the forcing frequency, or any frequency of interest, is used to reconstruct the vortical response at that frequency as in Equation 1:

$$\tilde{\omega}'_\theta(x,r,t) = \mathrm{Re}\left\{\hat{\omega}e^{i(2\pi ft)}\right\} \qquad (1)$$

The reconstructed fluctuating azimuthal vorticity in Equation 1 is a function of axial position, radial position, and time. It is calculated by taking the real component of the quantity $\hat{\omega}$ multiplied by the temporally-varying wave component. $\hat{\omega}$ is the complex, Fourier-transformed, azimuthal vorticity oscillation at the frequency of interest. The frequencies of interest in this study are the longitudinal acoustical forcing frequency for a given forcing condition, or any self-excited frequencies that are generated in the flow. This methodology has been used in previous studies for identifying key dynamics at the forcing frequency [28].

RESULTS

The flow field and its response to acoustic oscillations varies significantly with variations in swirl number and confinement. In this section, we describe the changes in flow and its response in three sections. First, we provide an overview of the time-averaged flow field. Next, we describe the effect of swirl number on azimuthal vorticity fluctuations. Finally, we describe the impact of confinement on some of these results.

Time-Averaged Flow Fields

Seven swirl numbers are examined in this study, generated with swirler blade angles of 0°, 15°, 30°, 40°, 50°, 57.5°, and 65°. The relationship between blade angle and geometric swirl number, as defined by Dunn-Rankin [31], is given in Appendix A. Variations in the swirl number result in significant changes to the time-averaged structure of the flow field. The first four blade angles were chosen to understand the addition of swirl without time-averaged vortex breakdown. At 50°, the effects of vortex breakdown and recirculation are studied. The transition to a PVC is observed at the 57.5° and 65° blade angles.

Figure 2 shows the time-averaged axial velocity profiles of the jet for each of the swirl conditions studied. For each of these swirl conditions, the maximum time-averaged axial velocity is located near the dump plane. Further downstream, the time-averaged axial velocity decreases, which can be attributed to jet spreading. The jet spreading increases as swirler blade angle is increased, which is expected [32], and can be seen in the axial velocity profiles in Figure 2.

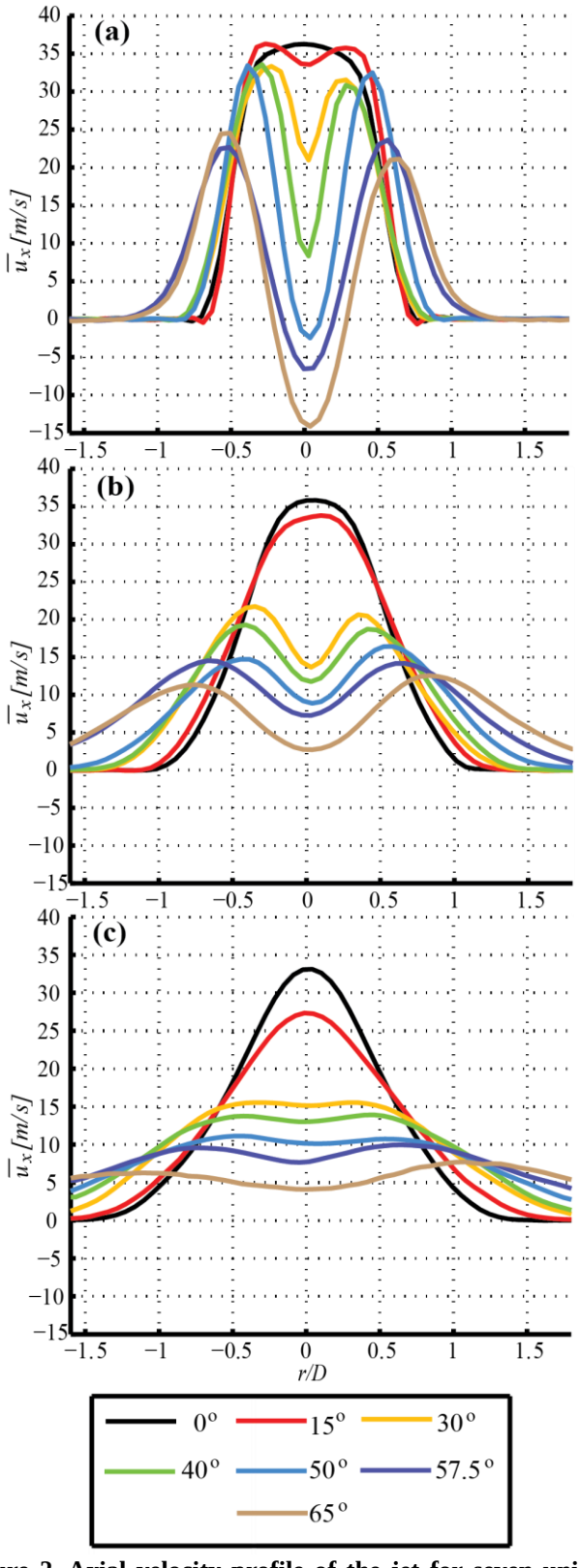

Figure 2. Axial velocity profile of the jet for seven unique swirl conditions at three downstream distances where (a) is *x/D*=1, (b) is *x/D*=3, and (c) is *x/D*=5.

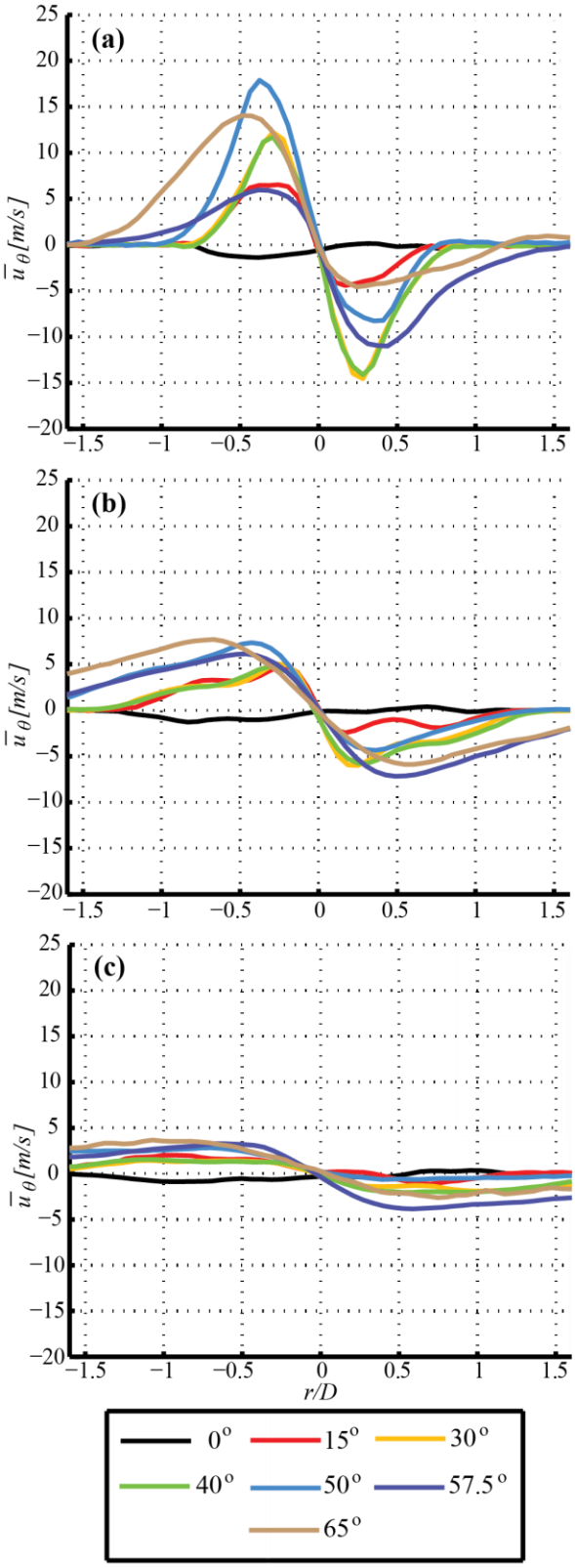

Figure 3. Azimuthal velocity profile of the jet for seven unique swirl conditions at three downstream distances where (a) is *x/D*=1, (b) is *x/D*=3, and (c) is *x/D*=5.

For the non-swirling jet, the axial velocity is maximum at the center and relatively uniform radially, exhibiting the expected axisymmetry around the centerline. As swirl is introduced, the jet begins to develop a "dip" in the time-averaged axial velocity along the centerline, which can be attributed to intermittent vortex breakdown. This dip in time-averaged axial velocity continues to increase as the swirler blade angle is increased. At blade angles of 50° and above, a negative time-averaged axial velocity appears at *x/D*=1 along the jet centerline. This negative centerline velocity is evidence of consistent vortex breakdown and the formation of a central recirculation zone in the jet at higher levels of swirl. The recirculation zone is strongest for the 65° swirl case. The jet spreading is also greatest at this swirl level. Specifically, at *x/D*=1, the increase in the jet spreading in comparison to the lower swirl levels is much greater for the 57.5° and 65° swirl cases. This is the portion of the flow field where the recirculation zone is located, and we will show later that at the 65° swirl level, and possibly even the 57.5° swirl level, a precessing vortex core (PVC) is present.

Figure 3 shows the time-averaged azimuthal velocity of the jet. For all swirl conditions, the highest time-averaged azimuthal velocity occurs at *x/D*=1. The non-swirling jet shows very little to no azimuthal velocity. As swirl is introduced, there is an increase in azimuthal velocity. At the 50° swirl level there is a peak in azimuthal velocity in the left hand portion of the jet. As swirl is increased further to the 57.5° and 65° swirl levels there is an apparent decrease in azimuthal velocity. This may seem counterintuitive; however, as mentioned previously, these cases (57.5° and 65°) display a precessing vortex core. As the PVC is a highly nonlinear phenomena, the instantaneous effect that it has on the flow may not be adequately represented by the time-averaged velocity profile. It is also worth noting that the flow is not axisymmetric at higher swirl numbers. This discrepancy can be explained by the fact that the introduction of swirl will generate non-axisymmetric behavior in the jet [33].

The time-averaged velocity of the flow is examined under three acoustic forcing conditions; acoustic forcing does not significantly alter the time-averaged flow structure relative to the unforced cases. In this work, we consider two forcing frequencies (600 Hz and 1800 Hz), and at 1800 Hz, we consider two forcing amplitudes. Initial linear stability analysis predicted the most amplified frequency of the non-swirling jet is 600 Hz, and so it is used as a baseline in this study. Additionally, these frequencies were chosen to be above and below the PVC frequency, 1033 Hz. We quantify the acoustic amplitudes by the non-dimensionalized $u_a'/\bar{u}$. These results are discussed later with reference to Figure 9.

Figure 4 shows a comparison of the time-averaged centerline velocity of the jet at 50° blade angle under no forcing, 600 Hz, 1800 Hz low amplitude, and 1800 Hz high amplitude forcing. There is agreement between the forced and unforced cases, and we see equivalent agreement when comparing the time-averaged centerline velocities of the forced

and unforced cases at all other swirl levels as well. From these comparisons, we can conclude that the acoustic forcing does not significantly alter the time-averaged structure of the jet.

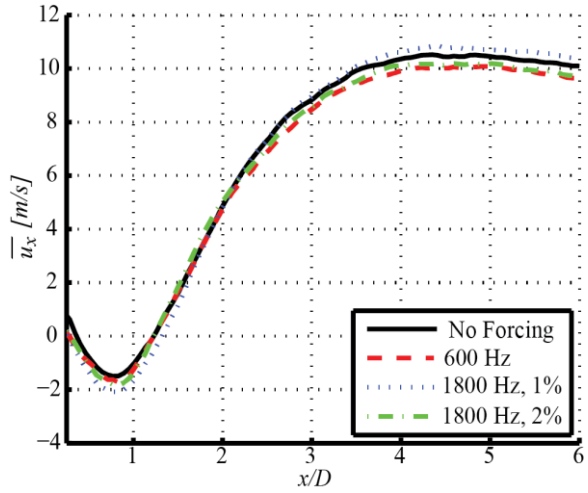

Figure 4. Time-averaged centerline velocity comparison of unforced jet to three acoustically-forced jets at a blade angle of 50°.

Effect of Swirl Number on Azimuthal Vorticity Fluctuations

This section describes the effect of swirl level on azimuthal vorticity fluctuations in order to evaluate how changes in swirl level influence the jet receptivity to longitudinal acoustic forcing. Figure 5 shows contour plots of one phase of the harmonic reconstruction of the fluctuating azimuthal vorticity at each forcing frequency and amplitude for six swirl cases between 0° and 57.5° swirler blade angles. The axial distances of x/D=0-4 are shown for the 600 Hz case and x/D=0-2 is shown for the 1800 Hz cases because the jet response downstream of these points is insignificant.

For the non-swirling jet case (0°), the 600 Hz forcing elicits a much different response than the 1800 Hz forcing. Under 600 Hz forcing, relatively weak vorticity fluctuations with peak magnitudes around 450 s^{-1} are convected downstream with a wavelength of approximately L^*=0.85D. This convective wavelength, L^*, is dependent on the forcing frequency and is relatively uniform across all swirl levels. Under 600 Hz forcing, the fluctuations begin to develop around x/D=1 and the peak vorticity fluctuation magnitude is located near x/D=2.5. With 1800 Hz forcing at 1% amplitude, the peak vorticity fluctuations in the non-swirling jet are relatively strong, 800 s^{-1}, and they convect downstream with a wavelength of approximately L^*=0.2D. The vorticity fluctuations develop much closer to the nozzle exit under 1800 Hz forcing than they do at 600 Hz forcing because the convective wavelength is shorter. With 1800 Hz forcing at 2% amplitude, the peak vorticity fluctuations are stronger, approximately 1400 s^{-1}, or twice as strong as those in the 1% forcing case. This indicates that the forcing is in the linear regime.

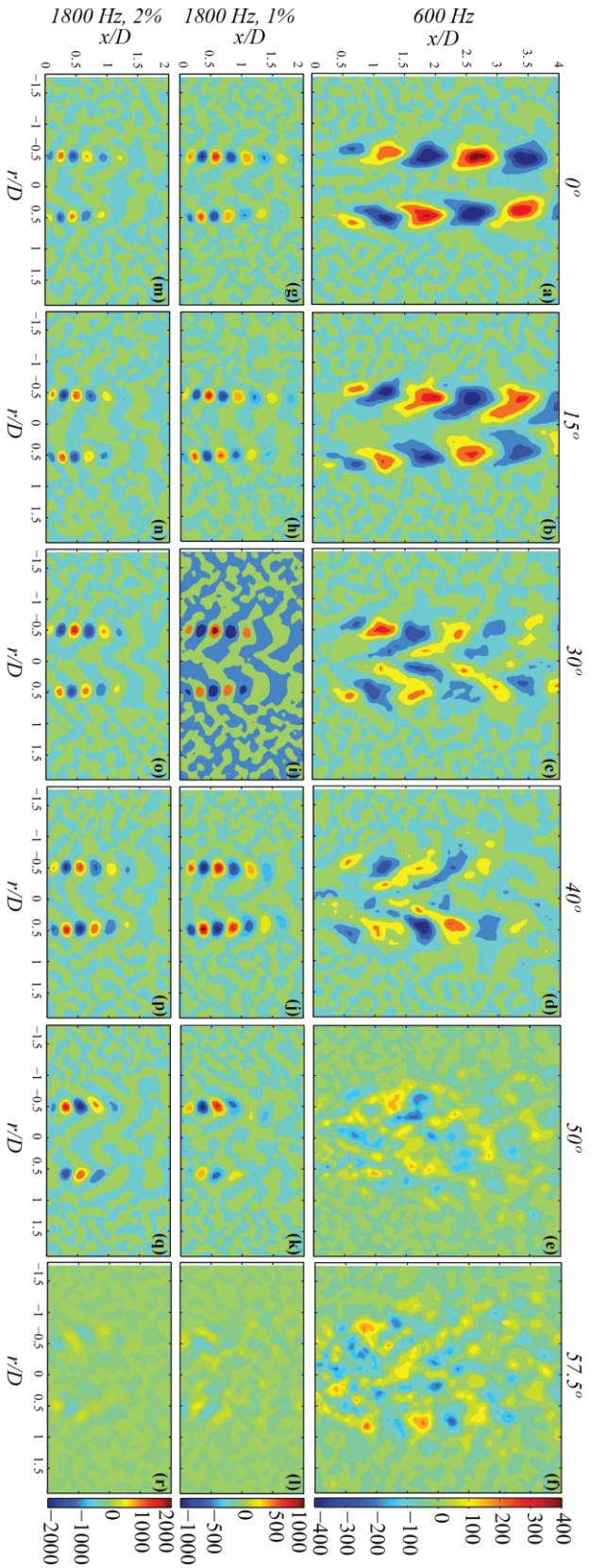

Figure 5. Harmonic reconstruction of fluctuating azimuthal vorticity response at the respective forcing frequency.

As swirl is introduced and increased, there are a number of noticeable changes in the vorticity response. There is diminishing coherence in the vortical response to 600 Hz acoustic forcing as swirl is increased. Between the 15° and 50° swirler blade angles, the jet transitions with the onset of vortex breakdown. There is no discernable pattern of vortex shedding in the harmonic reconstruction at swirler angles beyond 40° for 600 Hz forcing. One plausible explanation for this behavior is the presence of the vortex breakdown bubble. As it moves further upstream with increasing swirl, the shear layers are less responsive to 600 Hz forcing.

The 1800 Hz forcing cases have a very different vorticity response to acoustic forcing. From 0° to 40° swirler blade angles, the vorticity peaks develop very close to the dump plane and decay almost entirely by the axial distance x/D=1.5. For the 1800 Hz forcing cases, azimuthal vorticity peak magnitudes increase as swirl increases until the formation of a PVC at 57.5°. The peaks in vorticity magnitude increase to approximately 1000 s^{-1} for 1800 Hz 1% forcing and to 2000 s^{-1} for 1800 Hz 2% forcing when between a blade angles of 0° and 15°. As swirler blade angle is increased from 15° to 40°, there is very little change in the magnitude or location of the vorticity peaks for 1800 Hz forcing. For the 50° swirler blade angle case, the 1800 Hz forcing appears to decay sooner and the shear layer appears to grow wider relative to the lower swirl cases. This behavior could be explained by the vortex breakdown bubble and its movement further upstream with increasing swirl. This would induce more jet spreading and mean shear for the 50° swirler blade angle case in the region most receptive to the 1800Hz forcing.

At the 57.5° swirler angle, the 1800 Hz forcing elicits only very weak vortex shedding in the shear layers. The peak vorticity magnitudes are approximately an order of magnitude lower than was observed at the lower swirl levels. This drastic change in vorticity response between 50° and 57.5° swirler blade angle cases is most likely due to the formation of a PVC at 57.5°. The final swirl case 65° exhibits a fully developed PVC and essentially no response at the forcing frequency is present.

Acoustic Receptivity and the Describing Function

As mentioned in the previous section, the convective wavelength of the vorticity oscillations, L^*, is a function of the forcing frequency and convective speed of the flow. Figure 6 shows the amplitude of the vorticity fluctuations at the forcing frequency along the shear layer versus the normalized downstream distance (x/L^*) in the 15° case to further quantify the receptivity of the flow to different forcing conditions. Here, the maximum vorticity fluctuation occurs near x/L^*=2 and the decay rate of the vorticity fluctuations is relatively similar for all forcing conditions. This indicates that vortex formation and decay scale well with the convective wavelength across all forcing frequencies, as has been noted by O'Connor [34].

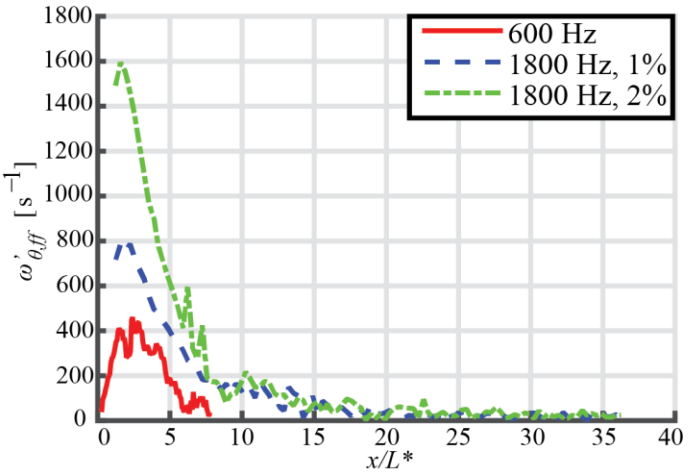

Figure 6. Receptivity comparison of three acoustic forcing conditons for the 15° swirl case.

The receptivity of the azimuthal vorticity fluctuations to acoustic excitation can be more precisely quantified through the use of a describing function, F_ω. The describing function, expressed in Equation 2, relates azimuthal vorticity fluctuations, ω_θ, to the incoming acoustic velocity perturbations, u'. The describing function is a function of the forcing frequency, f, the forcing amplitude, A, and the swirl number, S, as are the fluctuating azimuthal vorticity and acoustic velocity. While the results in Figure 5 clearly show that the fluctuating azimuthal vorticity is a function of the swirl number, we have also generalized the acoustic velocity perturbations to be a function of swirl number in order to account for variations in acoustic impedance of the swirler as the blade angle varies. The time-averaged vorticity and velocity fields are also a function of swirl number, but as shown in Figure 4, are not a function of the acoustic forcing amplitude or frequency at these conditions.

$$F_\omega(f,A,S) = \frac{\omega'_\theta(f,A,S) \,/\, \bar{\omega}(S)}{u'_a(f,A,S) \,/\, \bar{u}(S)} \qquad (2)$$

The vorticity fluctuation used in the describing function is calculated for a region in the flow field located in the shear layer at two convective wavelengths, $2L^*$, downstream for each forcing frequency. This area is chosen because the vorticity fluctuations are shown to be localized in the shear layers and as can be seen in Figure 6, x/L^*=2 is the region where the vorticity fluctuations are fully developed. The acoustic velocity fluctuations used in the describing function are calculated using the two microphone method.

Figure 7 shows the measurements of the normalized fluctuating azimuthal vorticity as a function of swirl number for each of the forcing conditions. The trends seen in the harmonic reconstructions in Figure 5 are reflected in the results in this figure. The vortical response to 600 Hz forcing decreases as

swirl increases. The response to 1800 Hz forcing increases as swirl increases from the 0° swirl angle to 15° and then remains relatively constant until the 50° swirl angle. In the 57.5° and 65° cases, there is a significant drop off in response to the 1800 Hz forcing as a result of the PVC. The apparent increase in response at 57.5° for the 600 Hz forcing can most likely be attributed to high levels of turbulence caused by the PVC.

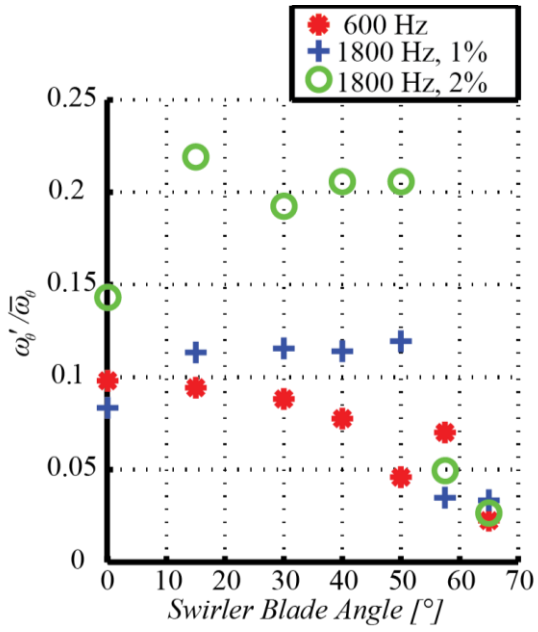

Figure 7. Fluctuating azimuthal vorticity response to acoustic forcing as a function of swirler blade angle.

To better quantify the coherence of the vortical fluctuations as compared to the turbulent fluctuations in the flow, a signal to noise ratio for the coherent fluctuating vorticity is shown in Figure 8. This signal to noise ratio is calculated by dividing the local fluctuating azimuthal vorticity at the forcing frequency, as shown in Figure 7, by the vorticity fluctuation level at the forcing frequency in an unforced case. The fluctuating vorticity amplitude at a given frequency in an unforced flow is generated by turbulence, meaning that it is incoherent, and is an estimate for the "noise floor" of the vorticity measurement. For all cases, the signal to noise ratio falls below 2 when the swirler angle is 50° or higher. This is further evidence that the vortical response at these higher swirl levels should not be attributed to the acoustic forcing, but instead to turbulence in the jet. There is also a significant drop in signal to noise ratio when the onset of PVC occurs.

Figure 9 shows the measurements of acoustic velocity fluctuation amplitudes in the nozzle as a function of swirl that are used to calculate the describing function. There is an increase in acoustic velocity fluctuation magnitude for all three forcing conditions as swirl increases. This change is likely due to variations in the swirler impedance as the open area of the swirler decreases with increasing blade angle. The signal to noise ratio for the nozzle velocity fluctuation is calculated for each forcing frequency at each level of swirl using the pressure spectra. On average, the signal to noise ratio is approximately 15:1 for 600 Hz forcing, 48:1 for 1800 Hz 1% forcing, and 106:1 for 1800 Hz 2% forcing. However, in the cases where a PVC was present (65°), the signal to noise ratio for the 600 Hz forcing is low as 1.3. This is due to the fact that the PVC is a self-excited phenomena that generates considerable "noise" at relatively a range of frequencies.

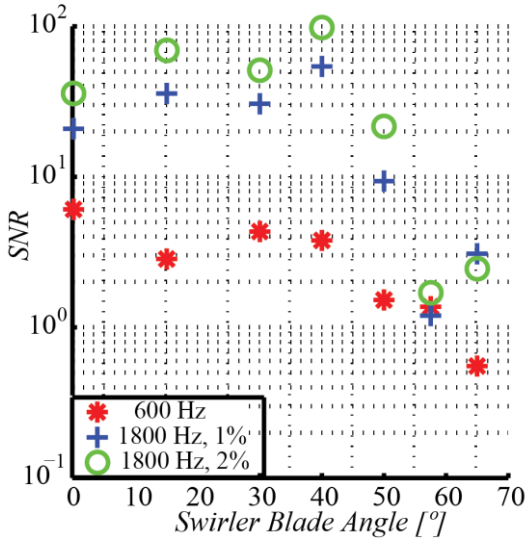

Figure 8. Signal to noise ratio for the fluctuating azimuthal vorticity response to acoustic forcing.

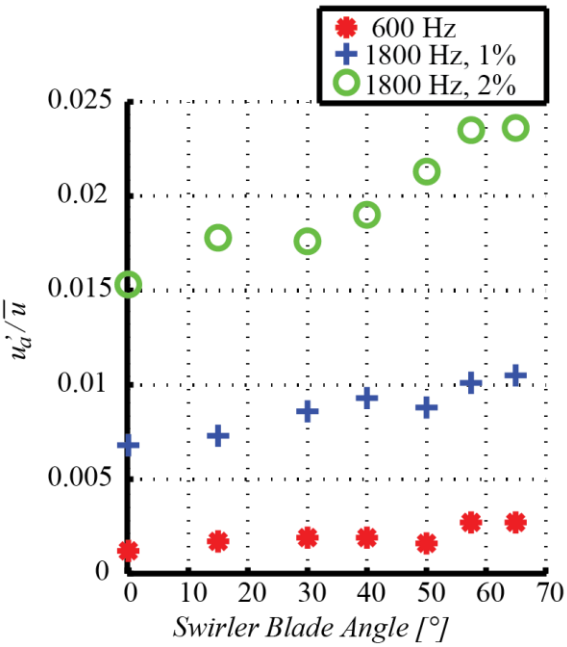

Figure 9. Measurements of the fluctuating acoustic velocity of a given forcing condition as a function of swirler blade angle.

Figure 10 shows the gain of the describing function, which relates the azimuthal vorticity fluctuations to the incoming longitudinally-forced, acoustic velocity fluctuations as a function of swirl. This describing function is a quantification of the receptivity of the shear layer to acoustic forcing. For 600 Hz forcing, the vortical response of the jet is quite significant at low levels of swirl, and there is a dramatic decrease in flow receptivity as the swirler blade angle is increased.

For 1800 Hz forcing, the receptivity is relatively constant for all swirl cases from blade angles of 0° to 50°. There is no increase in receptivity of the flow at the higher amplitude forcing level for 1800 Hz since both forcing amplitudes fall in the linear regime. After the formation of the PVC at a blade angle of 57.5°, the receptivity to 1800 Hz forcing decreases significantly. The describing function measurements are essentially zero for both the 1800 Hz forcing conditions at swirler blade angles of 57.5° and 65°.

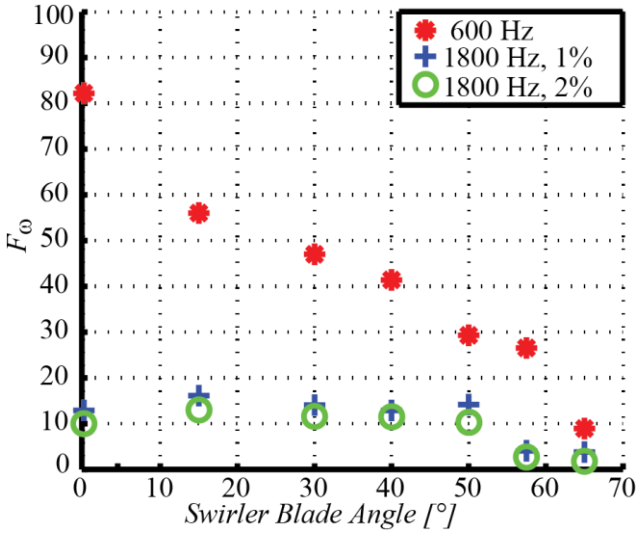

Figure 10. Vorticity describing function as a function of swirl number at two frequencies and two forcing amplitudes.

PVC Dynamics

Companion linear stability analysis has shown that above a blade angle of 50°, the flow field develops a global instability; for the sake of brevity, this analysis is not discussed in detail but follows that of Hansford *et al.* [35]. Both experiments and theory indicate that a PVC is present at 57.5° and 60° swirl angle. A PVC is a physical manifestation of a global mode in swirling flows, and is characterized by a high-amplitude helical oscillation in the vortex breakdown region. At sufficiently high swirl numbers, the flow becomes dominated by this nonlinear, limit-cycle oscillator, and the PVC significantly modifies shear layer acoustic receptivity in this flow field.

From Figure 7, the vorticity response at the forcing frequencies is small for the two highest swirl numbers. Instead, at the highest swirl number, most of the vortical fluctuations occur at 1033 Hz. Unlike the vorticity fluctuations caused by acoustics, these fluctuations are concentrated in the center of the flow field and are generated by the precessing vortex core. The vorticity fluctuations display a helical motion instead of an axisymmetric motion, as seen in the shear layer response in Figure 5. These traits indicate that a PVC is present. The PVC dominates the flow field and prevents the acoustic fluctuations from causing vortical rollup in the shear layers at the acoustic frequency; it reduces the receptivity of the shear layers.

Figure 11 shows the effect the PVC has on the dominant frequencies in the flow, as measured by the nozzle pressure transducer closest to the dump plane. This figure plots the linear spectrum for three different swirl cases with 1800 Hz forcing at 2% of the bulk nozzle velocity. The green line shows data from the 40° case; the 50° swirler angle case is shown in black, which has recirculation but no prominent PVC, and 65° is shown in red where a PVC is present. The PVC has a peak frequency near 1050 Hz and displays a much broader spectrum than the acoustics at 1800 Hz. As the swirl increases, the strength of the PVC increases and the pressure fluctuations at the forcing frequency are affected. For the highest swirl case, the PVC and acoustic pressure fluctuation amplitudes are nearly equal.

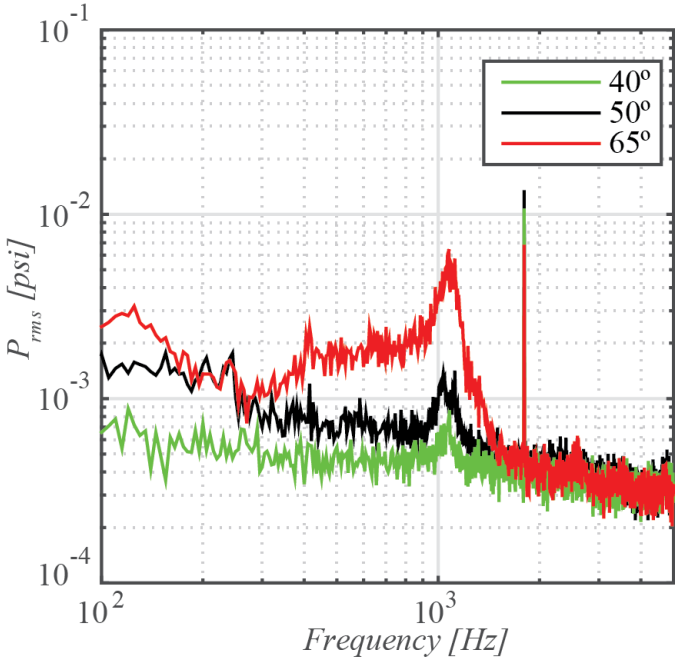

Figure 11. Linear spectrum from the near nozzle pressure transducer for three different flow fields showing the impact of a precessing vortex core on the acoustic pressure fluctuations.

A harmonic reconstruction of the vorticity fluctuation at the PVC frequency in the 1800 Hz, 2% forcing case is shown in Figure 12, where the amplitude of the vorticity fluctuation at the PVC frequency is significantly larger than that at the forcing frequency (see Figure 5). This indicates there is a complex, nonlinear coupling mechanism between the PVC, the flow, and the acoustic field, and the mechanism has both an amplitude and

frequency dependence. As a result, the PVC is capable of suppressing the shear layer response to acoustic forcing, resulting in a very low vorticity describing function gain at conditions with a PVC.

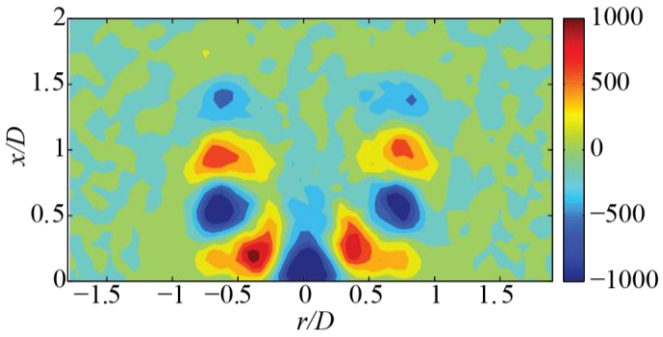

Figure 12. Vorticity reconstruction at the PVC frequency, 1071 Hz, when 1800 Hz forcing is applied at an amplitude of 2% the bulk nozzle velocity for a 65° swirler angle.

Effect of Confinement on Vorticity Fluctuations

Next we consider the effects of confinement at three different swirler angles, 15°, 50°, and 65°. These swirler angles were chosen because they represent canonically different flow states: 15° corresponds to a swirling jet with minimal central recirculation, 50° corresponds to a swirling jet with time-averaged vortex breakdown, and 65° corresponds to a swirling jet with a PVC. The confinement used is shown in Figure 1. The combustion chamber has a diameter of 13 cm, is 20.3 cm tall, and is made of fused quartz for optical accessibility. For this study, there is no contraction on top of the combustion chamber.

Confining the flow field introduces corner recirculation zones that are not seen in the unconfined flow. The downstream development of the jets are different when the flow field is confined. The time-averaged vorticity field with streamlines generated from the time-averaged axial and radial velocities are shown in Figure 13. At all swirler angles, the axial velocity at all radial positions is lower in the confined-flow cases than in the corresponding unconfined cases. Additionally, for the 15° swirler angle, the jet core diverts to the left side of the chamber. This becomes noticeable at x/D=3 and 5, and has been noted in other studies [36]. Even though great care is taken to ensure that the jet is vertical, the jet tilts starting around x/D=3 for this swirl angle, likely as a result of the weak yet uneven recirculation around the circumference of the jet. The jet impacts the wall and the flow travels back towards the nozzle exit along the wall.

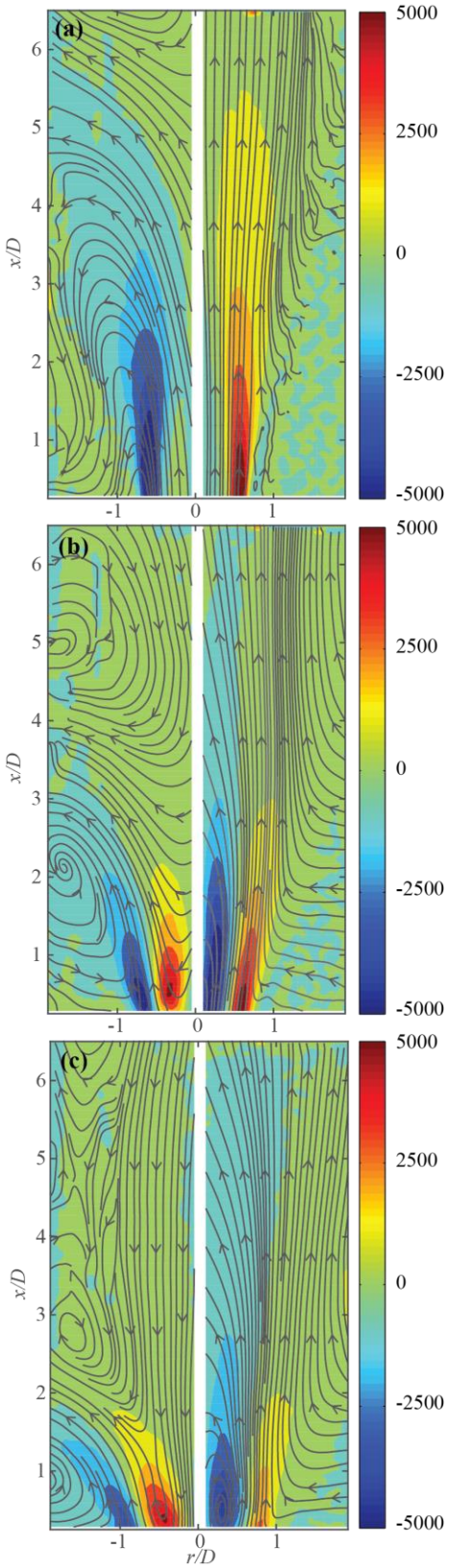

Figure 13: The time-averaged vorticity fields for both confined (left) and unconfined flow fields (right) for 15° (a), 50° is shown in (b), and 65° in (c).

At the two higher swirler angles, the jet spreads faster and the vortex breakdown bubble is significantly larger than in the unconfined cases. For a swirler angle of 50°, there is a small region of recirculation at x/D=3. At this downstream position, the jet impinges on the wall and flow travels along the wall towards both the dump plane and exhaust. Here, two distinct recirculation zones form along the chamber wall, unlike the unconfined cases where the jet entrains ambient air. As a result of these large recirculation regions, the shear layers are thicker and structures in the shear layer decay more quickly in the confined flow. These differences in the shear layer strength and thickness could have a significant effect on their receptivity to acoustic oscillations. At a swirler angle of 65°, the jet-wall impact region moves closer to the dump plane, with the recirculation zones located just above and below this impact region. The streamlines also show the extent of the size of the inner recirculation zone, which encompasses most of the flow field after jet impacts the wall.

Comparisons between vorticity fluctuations at the forcing frequency in the confined and unconfined flows are shown in Figure 14. This figure compares coherent vorticity fluctuations at three swirler angles and three acoustic forcing conditions. Across all vorticity fields, the coherent vorticity fluctuation amplitudes are weaker when there is confinement as compared to cases with the same acoustic forcing without confinement. When the swirler angle is 15°, the coherent vortical fluctuations at 600 Hz are significantly reduced. The response to both 1800 Hz forcing cases are weaker, but the differences between the confined and unconfined cases are not as significant as the differences for 600 Hz forcing. At the higher swirler angles, the response to acoustic oscillations is almost nonexistent. The shear layer response in the 50° blade angle case is coherent, yet weaker, at 1800 Hz; there is almost no coherent response at 600 Hz. At 65° blade angle, the harmonic reconstructions at 600 Hz and 1800 Hz are similarly random for the unconfined and confined cases, indicating that the PVC dominates the flow dynamics in both cases.

While not shown, the acoustic velocity fluctuations in the nozzle with and without confinement are similar. The characteristic vorticity fluctuations (taken at x/L^*=2) at the acoustic frequency normalized by the time-averaged vorticity are plotted in Figure 15(a). Compared to the unconfined flow cases, the vorticity fluctuations for the confined flows are lower. The 600 Hz and 1800 Hz 1% forcing cases have similar normalized vorticity fluctuations. The vorticity amplitude increases for these two forcing conditions between 15° and 50° while the response to 2% amplitude, 1800 Hz forcing decreases between these blade angles. Finally, at the 65° blade angle, the vortical response to both 1800 Hz forcing cases is small, while response to the 600 Hz increases.

The amplitude of the vorticity describing function, shown in Figure 15(b), shows similar trends for 1800 Hz forcing as that of the unconfined cases but opposite trends for 600 Hz forcing. Referring to Figure 13 (b, c), the vorticity fluctuations at 600 Hz are not coherent at the 50° and 65° swirler angles; therefore, the magnitude values given in Figure 15(b) for 600 Hz are non-physical. The amplitudes of the describing function in the 1800 Hz forcing cases display similar trends compared to their unconfined counterparts, albeit at lower magnitudes when confined. The recirculation zones appear to reduce the receptivity of the flow field to acoustic oscillations. On the whole, the receptivity to acoustic forcing is reduced when the flow field is confined.

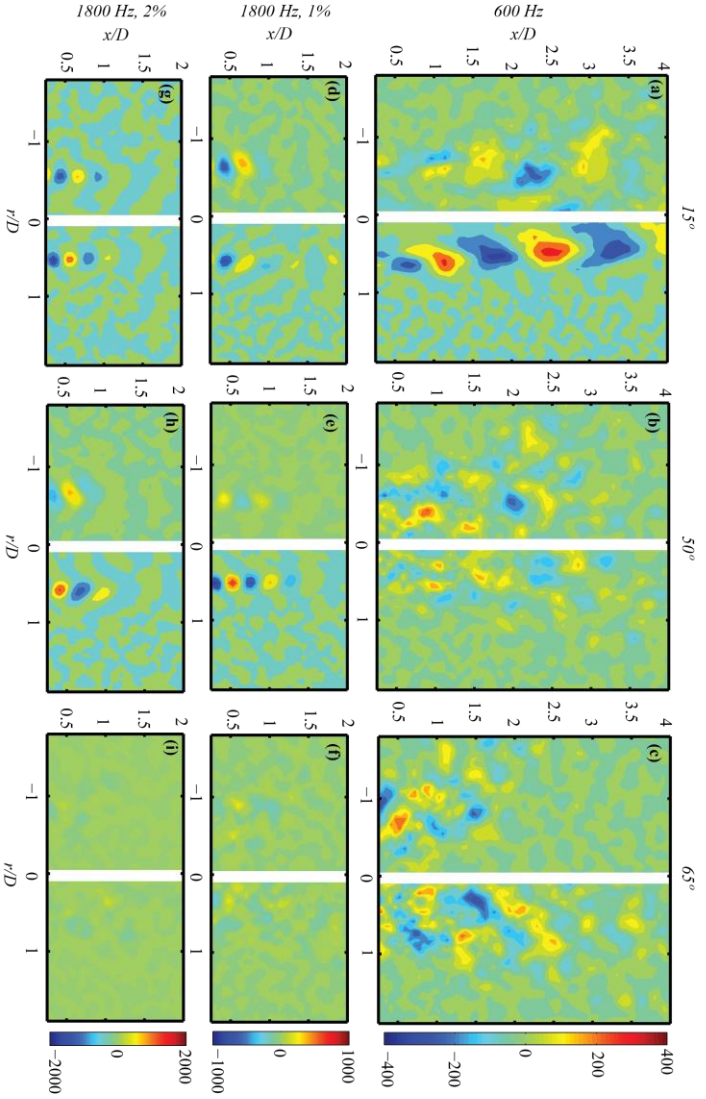

Figure 14: Vorticity response for confined (top) and unconfined (bottom) flows at a 15° (a, d, g), 50° (b, e, h), and 65° (c, f, i) swirler angle. Forcing is at 600 Hz (right), 1800 Hz at 1% forcing amplitude (center), and 1800 Hz at 2% forcing amplitude (left).

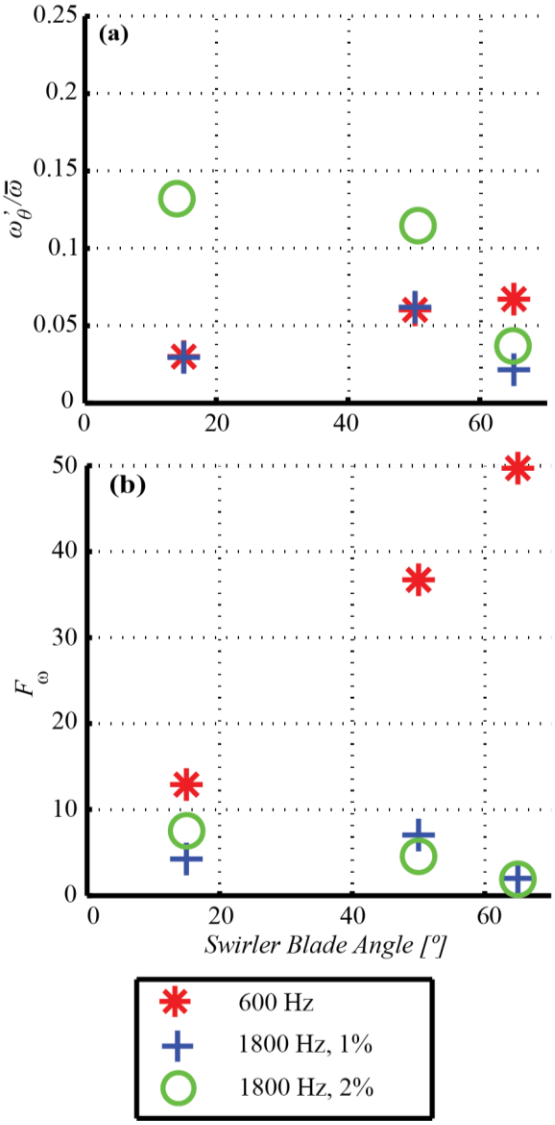

Figure 15: (a) The fluctuating vorticity response normalized by the time-averaged vorticity. (b) The describing function for three different confined swirl cases.

To determine if the vortical fluctuations that are shown in Figure 15(a) are the coherent response to acoustics, we compare the vorticity fluctuations in the forcing cases to the unforced vorticity fluctuations at the same frequency (as in the analysis in Figure 8). Comparing to the signal-to-noise values calculated in Figure 8, the SNRs in the confined cases are lower than the unconfined flows. The vorticity response is lower when there is confinement, and the SNR for all three 600 Hz forcing cases are less than or near unity. Therefore, the amplitude of the describing function for 600 Hz forcing cannot be considered to be due to acoustic forcing; the vortical fluctuations are driven mostly by turbulence. Even at the highest swirler angle, 65°, the SNR is no greater than 2. The response cannot be said to be due to acoustic oscillations for five out of the nine cases as a result of their low signal-to-noise ratio.

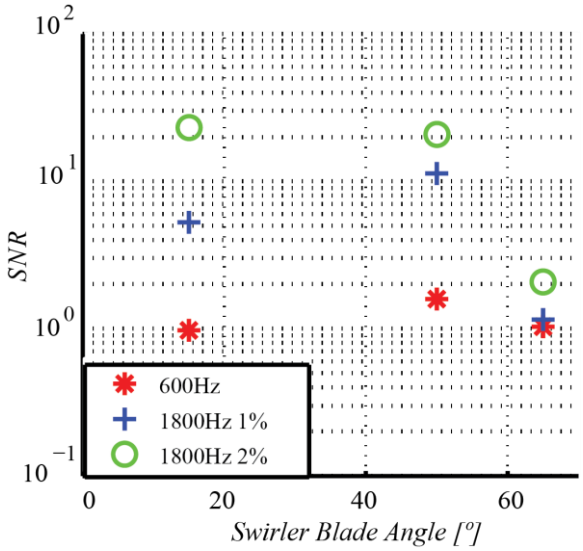

Figure 16: Signal-to-noise ratio for the fluctuating azimuthal vorticity response to acoustic forcing with confinement

Figure 17 shows the pressure spectra inside the nozzle for the confined cases in the 2% amplitude, 1800 Hz forcing cases at three swirl numbers. The pressure fluctuation amplitude at the forcing frequency increases with swirl number, as in the unconfined cases. However, the overall pressure fluctuation level is lower in the confined cases than in the unconfined cases. A strong PVC is present at 1006 Hz in the 65° case, and it acts to suppress the receptivity of the shear layers to acoustic forcing as in the unconfined case.

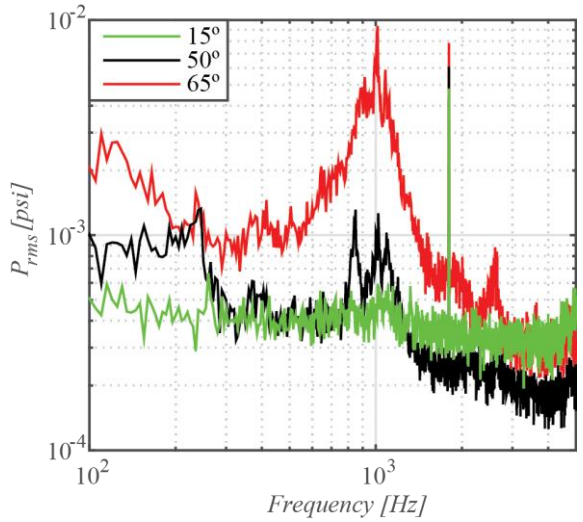

Figure 17: Pressure spectra for the three confined swirler angles undergoing 1800 Hz forcing at 2% amplitude with respect to the bulk nozzle velocity.

CONCLUSIONS

This study examines the relationship between acoustic forcing and vorticity response as a function of swirl number, shedding light on the important vorticity-coupling mechanism present during combustion instability. These data also suggest that confinement, or the significant changes to the flow field and shear-layer structure that confinement creates, can change the receptivity of the shear layers to acoustic forcing. Utilizing PIV and two pressure sensors along the injector, we determine the vorticity fluctuations and the acoustic velocity fluctuations, respectively. Using both of these quantities, a describing function is created. The time-averaged axial and azimuthal velocity profiles show the transition of the flow field from a non-swirling jet to a swirling jet with recirculation and a PVC. The forcing did not alter the time-averaged flow field but did significantly change the dynamic response. As the swirl number increases, the vorticity response to acoustic forcing decreases at 600 Hz and is finally suppressed in the presence of a PVC. When a PVC is present the response to 1800 Hz forcing is also reduced. When the flow field is confined, outer recirculation zones begin to form. The upstream outer recirculation zone alters the response to acoustic forcing because it significantly changes the structure of the shear layer.

These results have important implications for the flame response to various acoustic frequencies and amplitudes at different swirler angles. In particular, it has shown that a vorticity transfer function can be calculated and used to characterize the flow receptivity to acoustic fluctuations. This transfer function could have applications in reduced-order modeling, such as level set formulations [24], where a flow field is specified and the flame response is calculated. In future, one could measure the sensitivity of a given flow field to acoustic perturbations as a function of frequency, amplitude, and flow characteristics, and then use this information as input to a parameter study using reduced-order flame modeling methodologies.

Future work will focus on understanding the vorticity transformation processes present in the swirling flow. In this work, we have measured the azimuthal vorticity fluctuations, but the axial vorticity fluctuations are also an important coupling mechanism in flame response [12]. In addition to characterizing the axial vorticity fluctuations as a function of swirl number, these further data would help characterize a “vorticity budget,” or distribution of acoustically-excited vorticity into its three components, as a function of both flow and acoustic characteristics. This budget could also be used as inputs to more accurate, three-dimensional reduced-order flame simulations.

ACKNOWLEDGMENTS

We would like to acknowledge our technologist, Larry Horner. The first author acknowledges The Pennsylvania State University Office of Undergraduate Education for providing funding for this project through the Erickson Discovery Grant Program in the summer of 2015.

APPENDIX A

Table 1 shows the geometry swirl number, following Dunn-Rankin [31], that corresponds to each blade angle quoted in the text.

Table 1: Relationship between the swirler blade angle and geometric swirl number.

Blade Angle (°)	Geometric Swirl Number
0	0.00
15	0.18
30	0.38
40	0.56
50	0.79
57.5	1.05
65	1.43

REFERENCES

1. Lieuwen, T.C. and V. Yang, (2013) *Gas turbine emissions*, Cambridge University Press, New York, NY
2. Rayleigh, J.W.S.B., (1896) *The theory of sound*, 2 Macmillan,
3. Lieuwen, T.C. and V. Yang, eds. (2005) *Combustion instabilities in gas turbine engines: Operational experience, fundamental mechanisms and modeling*. Progress in Astronautics and Aeronautics, ed. F.K. Lu, Vol. 210. American Institute of Aeronautics and Astronautics: Reston, VA
4. Ducruix, S., T. Schuller, D. Durox, S. Candel, (2003) "Combustion dynamics and instabilities: Elementary coupling and driving mechanisms" Journal of Propulsion and Power, **19**(5):722-734
5. Altay, H.M., R.L. Speth, D.E. Hudgins, A.F. Ghoniem, (2009) "Flame–vortex interaction driven combustion dynamics in a backward-facing step combustor" Combustion and Flame, **156**(5):1111-1125
6. McManus, K., U. Vandsburger, C. Bowman, (1990) "Combustor performance enhancement through direct shear layer excitation" Combustion and Flame, **82**(1):75-92
7. Poinsot, T.J., A.C. Trouve, D.P. Veynante, S.M. Candel, E.J. Esposito, (1987) "Vortex-driven acoustically coupled combustion instabilities" Journal of Fluid Mechanics, **177**:265-292
8. Emerson, B., J. O’Connor, M. Juniper, T. Lieuwen, (2012) "Density ratio effects on reacting bluff-body flow field characteristics" Journal of Fluid Mechanics, **706**:219-250
9. Shanbhogue, S., D.-H. Shin, S. Hemchandra, D. Plaks, T. Lieuwen, (2009) "Flame-sheet dynamics of bluff-body stabilized flames during longitudinal acoustic forcing" Proceedings of the Combustion Institute, **32**(2):1787-1794

10. Lespinasse, F., F. Baillot, T. Boushaki, (2013) "Responses of V-flames placed in an HF transverse acoustic field from a velocity to pressure antinode" Comptes Rendus Mécanique, **341**(1):110-120
11. Shanbhogue, S.J., S. Husain, T. Lieuwen, (2009) "Lean blowoff of bluff body stabilized flames: Scaling and dynamics" Progress in Energy and Combustion Science, **35**(1):98-120
12. Palies, P., D. Durox, T. Schuller, S. Candel, (2010) "The combined dynamics of swirler and turbulent premixed swirling flames" Combustion and Flame, **157**(9):1698-1717
13. Steinberg, A., I. Boxx, M. Stöhr, C. Carter, W. Meier, (2010) "Flow–flame interactions causing acoustically coupled heat release fluctuations in a thermo-acoustically unstable gas turbine model combustor" Combustion and Flame, **157**(12):2250-2266
14. O'Connor, J. and T. Lieuwen, (2012) "Further characterization of the disturbance field in a transversely excited swirl-stabilized flame" Journal of Engineering for Gas Turbines and Power, **134**(1):011501
15. Venkataraman, K., L. Preston, D. Simons, B. Lee, J. Lee, D. Santavicca, (1999) "Mechanism of combustion instability in a lean premixed dump combustor" Journal of Propulsion and Power, **15**(6):909-918
16. Huang, Y. and V. Yang, (2004) "Bifurcation of flame structure in a lean-premixed swirl-stabilized combustor: transition from stable to unstable flame" Combustion and Flame, **136**(3):383-389
17. Hauser, M., Lorenz, M., Sattelmayer, T., (2010) "Influence of Transversal Acoustic Excitation of the Burner Apporach Flow on the Flame Structure" ASME Turbo Expo 2010: Power for Land, Sea and Air, Glasgow, UK
18. Paschereit, C.O., Gutmark, E., Weisenstein, W., (2000) "Excitation of Thermoacoustic Instabilities by Interaction of Acoustics and Unstable Swirling Flow" AIAA Journal, **38**(6):1025-1034
19. Preetham, H. Santosh, T. Lieuwen, (2008) "Dynamics of laminar premixed flames forced by harmonic velocity disturbances" Journal of Propulsion and Power, **24**(6):1390-1402
20. Preetham., S.K. Thumuluru, T. Lieuwen, H. Santosh, (2010) "Linear response of laminar premixed flames to flow oscillations: unsteady stretch effects" Journal of Propulsion and Power, **26**(3):524-532
21. Shreekrishna, T.L. and T. Lieuwen, (2009) "High frequency premixed flame response to acoustic perturbations" 15th AIAA/CEAS Aeroacoustic Conference, Miami, FL,
22. Hirsch, C., D. Fanaca, P. Reddy, W. Polifke, T. Sattelmayer, (2005) "Influence of the swirler design on the flame transfer function of premixed flames" ASME Turbo Expo 2005: Power for Land, Sea, and Air, Reno, NV
23. Bunce, N.A., B.D. Quay, D.A. Santavicca, (2014) "Interaction between swirl number fluctuations and vortex shedding in a single-nozzle turbulent swirling fully-premixed combustor" Journal of Engineering for Gas Turbines and Power, **136**(2):021503
24. Acharya, V., D.-H. Shin, T. Lieuwen, (2012) "Swirl effects on harmonically excited, premixed flame kinematics" Combustion and Flame, **159**(3):1139-1150
25. Acharya, V. and T. Lieuwen, (2015) "Effect of azimuthal flow fluctuations on flow and flame dynamics of axisymmetric swirling flames" Physics of Fluids (1994-present), **27**(10):105106
26. Ho, C.-M. and P. Huerre, (1984) "Perturbed free shear layers" Annual Review of Fluid Mechanics, **16**(1):365-422
27. Durox, D., J.P. Moeck, J.-F. Bourgouin, P. Morenton, M. Viallon, T. Schuller, S. Candel, (2013) "Flame dynamics of a variable swirl number system and instability control" Combustion and Flame, **160**(9):1729-1742
28. O'Connor, J. and T. Lieuwen, (2011) "Disturbance field characteristics of a transversely excited burner" Combustion Science and Technology, **183**(5):427-443
29. Åbom, M. and H. Bodén, (1988) "Error analysis of two-microphone measurements in ducts with flow" The Journal of the Acoustical Society of America, **83**(6):2429-2438
30. Melling, A., (1997) "Tracer particles and seeding for particle image velocimetry" Measurement Science and Technology, **8**(12):1406
31. Dunn-Rankin, D., (2011) *Lean combustion: technology and control*, Academic Press, Burlington, MA
32. Liang, H. and T. Maxworthy, (2005) "An experimental investigation of swirling jets" Journal of Fluid Mechanics, **525**:115-159
33. Oberleithner, K., C. Paschereit, I. Wygnanski, (2014) "On the impact of swirl on the growth of coherent structures" Journal of Fluid Mechanics, **741**:156-199
34. O'Connor, J., (2015) "Visualization of Shear Layer Dynamics in a Transversely Forced Flow and Flame" Journal of Propulsion and Power, **31**(4):1127-1136
35. Hansford, S., J. O'Connor, K. Manoharan, S. Hemchandra, (2015) "Impact of Flow Non-Axisymmetry on Swirling Flow Dynamics and Receptivity to Acoustics" ASME Turbo Expo 2015, Montreal, Quebec
36. Zhiyao, Y., G.B. Isaac, S. Michael, L. Oliver, M. Wolfgang, (2016) "Investigation of Confined Turbulent Jet Flames Using kHz-Rate Diagnostics" doi:10.2514/6.2016-0185, 54th AIAA Aerospace Sciences Meeting, San Diego, CA